Check for updates

ADVANCED FUNCTIONAL MATERIALS
www.afm-journal.de

Electronic Delocalization Engineering of β-AsP Enabled High-Efficient Multisource Logic Nanodevices

Fangqi Liu, Tongtong Wang, Qiang Yu, Zixin Yang, Jingxian Xiong, Xiaolin Zhang, Pengwei Gong, Hongzhen Lin, Jian Wang, Sicong Zhu,* and Jian Wu**

Delocalized electron and phonon structures are directives for rationally tuning the intrinsic physicochemical properties of 2D materials by redistributing electronic density. However, it is still challenging to accurately manipulate the delocalized electron and systematically study the relationships between physiochemical properties and practical nanodevices. Herein, the effects of delocalized electrons engineering on blue-arsenic-phosphorus (β-AsP)-based practical devices are systematically investigated via implementing vacancies or heteroatom doping. A tendency of carrier conductivity property from "half-metal" to "metal" is initially found when tuning the electronic structure of β-AsP with adjustable vacancy concentrations below 2 at% or above 3 at%, which can be ascribed to the introduction of delocalized electrons that cause asymmetric contributions to the electronic states near the implementation site. In optical logic device simulations, broadband response, triangular wave circuit system signal, and reverse polarization anisotropy are achieved by adjusting the vacancy concentration, while extinction ratios are as high as 1561. The electric and thermic-logic devices realize the highest available reported giant magnetoresistance (MR) up to 10^{13}% and 10^{39}% at vacancy concentrations of 1.67% and 0.89%, respectively, which is significantly superior to the reports. The results shed light on the electronic delocalization strategy of regulating internal structures to achieve highly efficient nanodevices.

1. Introduction

Nanoelectronics devices, magnetic random-access memory (MRAM), photodetectors, transistors, and others are in high demand due to their relatively low energy consumption and highly efficient data transmission, which have been successfully fabricated and widely applied in energy, medicine, and communication science fields.[1–5] Thanks to the outstanding tunability of electrical, mechanical, chemical, optical, magnetic, and optoelectronic properties, 2D materials can reduce the short-channel effect of nanodevices while endowing them with excellent mechanical and flexible properties.[6–9] However, devices made up of single pristine 2D materials cannot satisfy multi-functional demands. Black phosphorus (BP), a 2D graphene successor, is widely used in the development of various functional devices in the laboratory due to its excellent and abundant physical and chemical properties.[10,11] But the BP fails to instability when exposed to the air atmosphere, limiting its further development. Recently,

F. Liu, T. Wang, X. Zhang, P. Gong, S. Zhu
Hubei Province Key Laboratory of Systems Science in Metallurgical Process
The State Key Laboratory for Refractories and Metallurgy
Collaborative Innovation Center for Advanced Steels
International Research Institute for Steel Technology
Wuhan University of Science and Technology
Wuhan 430081, China
E-mail: sczhu@wust.edu.cn

F. Liu, X. Zhang
Key Laboratory of Artificial Micro- and Nano-structures of Ministry of Education and School of Physical and Technology
Wuhan University
Wuhan 430072, China

The ORCID identification number(s) for the author(s) of this article can be found under https://doi.org/10.1002/adfm.202312830

© 2024 The Authors. Advanced Functional Materials published by Wiley-VCH GmbH. This is an open access article under the terms of the Creative Commons Attribution License, which permits use, distribution and reproduction in any medium, provided the original work is properly cited.

DOI: 10.1002/adfm.202312830

Q. Yu, Z. Yang, J. Xiong, J. Wu
College of Advanced Interdisciplinary Studies
National University of Defense Technology
Changsha 410073, China
E-mail: wujian15@nudt.edu.cn

Q. Yu, H. Lin, J. Wang
i-Lab & Key Laboratory of Nanodevices and Applications & Key Laboratory of Nanophotonic Materials and Devices, Suzhou Institute of Nano-Tech and Nano-Bionics
Chinese Academy of Sciences
Suzhou 215123, China
E-mail: jian.wang@kit.edu

P. Gong
Shanghai Key Laboratory of Special Artificial Microstructure Materials and Technology and School of Physics Science and Engineering
Tongji University
Shanghai 200092, China

J. Wang
Helmholtz Institute Ulm (HIU)
D89081 Ulm, Germany

as a derivative of BP, the successful fabrication of the binary alloy black arsenic phosphorus with ultimate stability [12–16] has inspired the study of another stable phase of blue arsenic phosphorus (β-AsP).[17,18] β-AsP has demonstrated the succeeding merits of extremely high carrier mobility (electron mobility of 10 000 $cm^2 V^{-1} s^{-1}$) and flexible electronic structure tunability.[19,20] For example, the β-AsP-based heterojunctions endow high efficiency in solar energy conversion or hydrolysis catalysis. However, the non-magnetic behavior and indirect band gap of β-AsP hinder its application in optoelectronic and spintronic devices. As expected, materials with easily tunable internal electrons and phonons can easily change their intrinsic properties targeting functional devices. Therefore, modifying and regulating β-AsP is the key to further development and improvement.

Recently, electronic delocalization has been widely recognized as an essential and valid strategy to tune the electronic states and phonon structure.[13,21–23] Defect and doping engineering are currently available as an extremely effective tool for constructing delocalized electrons. The introduction of a low concentration of transition metal (TM) atoms and vacancies can bring a disorder of electronic density in a limited local region and break the symmetry of electronic distribution in 2D materials, leading to a dramatic variation in physical and chemical properties.[24–27] In particular, rational construction of defects or implementing vacancy engineering on 2D materials can endow the targeted transformations of material properties and increase the high-performance output of their nanodevices, a long-sought golden standard in materials science.[28–30] For example, the trapping rate and Auger recombination rate of photo carriers are accelerated after adjusting the vacancy concentrations in a Bi_2O_2Se-based photonics device, further achieving a high-performance mode-locked laser.[31,32] Current understanding and strategies do not allow for resolving waste heat generation during the operation of nanodevices. Moreover, thermoelectric materials enable the effect to offer a direct way to transform heat energy into electric energy. In a new-emerging spin caloritronic field, incorporating the benefits of both thermoelectric and spintronics is attracting huge interest owing to its promising future in green energy and information science.[33–35] In terms of transformation efficiency, the conversion sites in thermoelectric materials seem to be of significance and provide opportunities to improve the efficiency of the recovery of waste heat from thermoelectric devices.[36] Taking all into consideration, developing a high electronic transfer and conversion efficiency based on 2D materials becomes more urgent for nanodevices, which have not been comprehensively studied.

In this work, the effects of delocalized electrons engineering on β-AsP-based practical devices are systematically investigated via introducing TM atom doping and vacancies inside β-AsP. This electron delocalization engineering well-modulates the local electronic density structure of β-AsP, especially the vacancy-induced electron delocalization that can realize the directional electrical property transition and displays a volcano tendency. The detailed functions and involved mechanisms are further investigated when applied to devices. In the optic-logic devices based on optimal β-AsP, the variation of vacancy concentration is capable of achieving regular modulation of polarization direction and triangular wave photoelectric response signal output (also implemented encode digital information as "1" and "0") of optoelectronic devices. Given the waste energy recovery during operations of electrical devices, the logic devices based on β-AsP electronically and thermally controlled magnetic tunnel junctions (MTJ) realize the highest available reported giant tunnel magnetoresistance (TMR) up to and colossal heat-induced magnetoresistance (HIMR) of 10^{39} at a vacancy concentration of 1.67% and 0.89%, respectively, while the 100% spin-filtering effect (SFE) remains unchanged with the vacancy concentration, significantly better than previous reports, accomplishing waste energy recovery of the nanodevice. Meanwhile, the thermal spin Hall effect is generated, realizing the concentration-controlled switching from pure charge flow to pure spin flow. These results imply the bright future of β-AsP with electronic delocalization in practical nanodevices for achieving high efficiency.

2. Results and Discussion

2.1. Model Designs of Delocalized Electron Engineering

All calculations of the electronic structure for materials and transport properties for devices are based on first principles calculations combining nonequilibrium Green's function (NEGF) by implementing in the Vienna ab initio simulation package (VASP),[37,38] Nanodcal,[39] and the Quantum ATK [40] software package (see details in Section S7, Supporting Information). Defects and heteroatom doping are two typical strategies employed experimentally and theoretically to significantly modulate the properties of materials. Herein, we implemented the substitution of TM elements on β-AsP in comparison with the vacancy treatment as a regulation effect. Initially, the crystal structure of β-AsP is constructed by substituting TM atoms for As and P atoms (3.1%) and introducing different concentrations of As and P atomic vacancies (1%–5.6%). For structures that are optimized for the implementation of vacancies, the structures implemented in the P vacancy keep stable as well, indicating the coexistence feasibility of the β-AsP with P vacancies (Figure S1a, Supporting Information). Meanwhile, according to surrounding molecular dynamics simulations, these β-AsP systems with vacancies were further assessed under different high temperatures (300, 500, and 700 K) (Figure S1b, Supporting Information). The potential energy in these systems remains stable at the ps-level, proving the feasibility of vacancy engineering (see details in Section S1, Supporting Information).

The electronic distribution structures of β-AsP with different TM atom substitution and vacancy concentrations are shown in Figure S2 (Supporting Information). The β-AsP can achieve various electronic property transitions under vacancy and substitution engineering. Surprisingly, a stable transition of β-AsP electrical properties can be achieved when the vacancy concentration is above or below a certain value (2.5%). The β-AsP exhibits continuously non-magnetic metallicity at high solubility vacancies and yields a distinct Dirac cone energy band below the Fermi energy level, which will significantly increase the carrier mobility. Whereas, the β-AsP shows consistently half-metallic at low

S. Zhu
Department of Mechanical Engineering
National University of Singapore
Singapore 117575, Singapore

© 2024 The Authors. Advanced Functional Materials published by Wiley-VCH GmbH

16163028, 0, Downloaded from https://onlinelibrary.wiley.com/doi/10.1002/adfm.202312830 by Karlsruher Institut F., Wiley Online Library on [13/08/2024]. See the Terms and Conditions (https://onlinelibrary.wiley.com/terms-and-conditions) on Wiley Online Library for rules of use; OA articles are governed by the applicable Creative Commons License

16163028, 0, Downloaded from https://onlinelibrary.wiley.com/doi/10.1002/adfm.202312830 by Karlsruher Institut F., Wiley Online Library on [13/08/2024]. See the Terms and Conditions (https://onlinelibrary.wiley.com/terms-and-conditions) on Wiley Online Library for rules of use; OA articles are governed by the applicable Creative Commons License

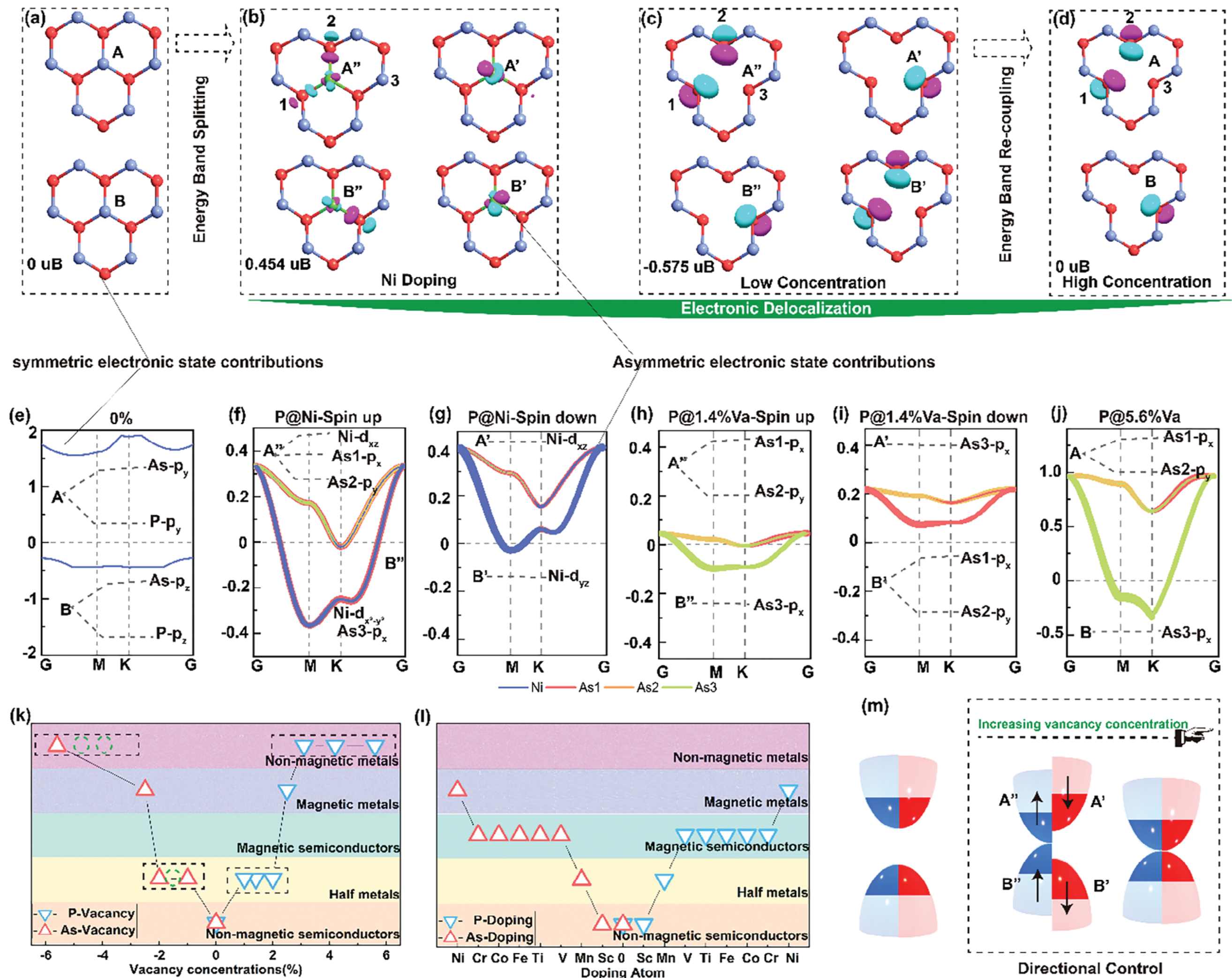

Figure 1. Regularized modulation and mechanism. The modulation of the electronic structure for β-AsP under various P-atom vacancy concentration engineering. MPSH of state A (spin up), state B (spin up), state A′ (spin down) and state B′ (spin down) at a) pristine, b) doped TM Ni atoms, c) 1% P-atom vacancies concentration and d) 5.6% P-atom vacancies concentration for β-AsP. Electronic band structure for β-AsP at e) pristine, f-g) doped TM Ni atoms, h-i) 1.4% and j) 5.6% P-atom vacancy concentrations. Intrinsic properties of β-AsP at different k) P(As) atomic vacancy concentrations and l) different TM atomic doping. m) Schematic diagram of the shift in the electronic state of β-AsP at TM atom doping and vacancy engineering.

concentrations of vacancies, which act as an ideal material for spintronic devices. As for the TM substitution, although the modulation of all-electrical properties can also be achieved, the modulation and fabrication seem too hard, while only TM - Mn substitution can modulate β-AsP into a half-metal. From the modulation effect, it can also be seen that the implementation of doping and defect engineering for both As and P atoms show the same effect of modulation, so it can be inferred that β-AsP is an equivalently isotropic material concerning As and P atoms (see details in Section S2, Supporting Information).

To better understand the vacancy modulation on the electronic structures of β-AsP, the wave function of the corresponding defect state is carried out. It is evident from the molecular projected self-consistent Hamiltonian (MPSH) that the electronic orbital contributions of A and B after the introduction of doping or vacancies mainly originate from the replacement atoms and the three As atoms closest to the implementation site, and an increase in the delocalization of the electrons can be observed (**Figure** 1a–d). This delocalization also causes A and B to move closer to the Fermi energy level in all modulation cases. The analysis of the band structure after defect engineering modulation also reveals that the electronic structure change of β-AsP is realized due to the shift and splitting of the conduction band (A) and valence band (B) closest to the Fermi energy level, so the following mechanism analysis mainly focuses on these two bands. The substitution of Ni atoms for P atoms makes β-AsP from a nonmagnetic semiconductor to a magnetic metal (Figure 1e–g). Both A and B split into a spin-up state (A′, B′) and a spin-down state (A″, B″), yielding spin polarization. Similar phenomena occur in the low-concentration vacancy situation, but no splitting takes place for A and B in the high-concentration vacancy engineering (Figure 1h–j). It can be seen from the energy bands of

© 2024 The Authors. Advanced Functional Materials published by Wiley-VCH GmbH

the primordial β-AsP that A is farther away from the Fermi energy level, which is mainly contributed equally by the p_y orbitals of As and P atoms. In comparison, B is closer to the Fermi energy level, dominated equally by the p_z orbitals of As and P atoms. Also consistent with our earlier speculation, β-AsP is a material about the equivalence of As and P atoms. A deeper explanation in terms of electron orbital contributions is required to further explain the mechanism of this phenomenon. It can be found that the spin-up and spin-down states of β-AsP are subjected to different electronic orbital contributions for Ni doping and under low concentration vacancies, which in turn leads to spin splitting of A and B. This is due to the poor symmetry of the crystal structure when interacting with other atoms or constructing low concentrations of vacancies, resulting in more electron delocalization near the doping or vacancy sites. In addition, although TM doping can significantly modulate the electronic structure of AsP, the diversity of d orbitals of the TM may lead to an irregular modulation (Figure 1k–m) (see details in Section S3, Supporting Information).

2.2. Delocalized Electron Engineering of β-AsP in Logic Nanodevices

Aiming to test further the boosting effect of this electron delocalization on applications, we designed three types of multi-source logic devices for applications varying from photodetectors, MTJ, and waste energy recovery based on β-AsP with doping and defect modulation. The photocurrent varies in a sinusoidal curve with the angle of polarization for photon energies, as is typical of the photogalvanic effect (PGE) (Figure S4a–c, Supporting Information). First of all, the photodetectors based on β-AsP with Mn doping or different vacancy concentrations are constructed as shown in **Figure 2a**. The previous electronic structure analysis shows that Mn@β-AsP exhibits a half-metallic property, with a spin-up state crossing the Fermi energy level and a spin-down displaying a low-energy-gap semiconductor property. As a result, the photovoltaic device exhibits a spin-up current in the low photon energy interval, and the spin-up current does not conduct, which demonstrates a perfect SFE. Compared to the pristine β-AsP devices with maximum photonic response in the visible range (VIS), the photonic response of the Mn@β-AsP device is significantly shifted towards the mid-infrared region (MIR) (Figure 2b). The low-concentration vacancy-modulated electronic structure has a similar effect to Mn-doping showing perfect spin efficiency at low photon energies but exhibiting excellent logical circuit system signals (Figure 2c). In contrast, the response of β-AsP devices under high-concentration vacancy modulation is significantly enhanced and the response range is significantly broadened, with strong responses in both the near- and far-infrared. The reason lies in the fact that a Dirac cone is generated near the Fermi energy level under the high concentration of vacancies, and the electronic conductivity is enhanced. Another criterion for evaluating photodetectors is polarization sensitivity. As the irradiation energy increases, the devices with pristine β-AsP structure exhibit strong polarization in the Y direction; while under low vacancy concentration, it is concentrated in the X direction. Increasing the vacancy concentrations, the devices exhibit isotropic polarization (Figure 2d–f), suggesting that vacancies can be employed as an extremely promising strategy for effectively tuning the performances of β-AsP -based optoelectronic devices. As well, the extinction ratio is another important index to evaluate the polarization sensitivity of photodetector devices. The extinction ratio (ER) of photovoltaic devices based on perfect β-AsP can be as high as 1561 when the photon energy is set as 1.8 eV (Figure S4d, Supporting Information), which is extremely higher than existing reports on 2D materials (Figure 4i). All these also indicate that β-AsP is an extremely promising target that can be used as a photodetector. For further information, see Section S4 of the Supporting Information.

Layered materials with half-metal characteristics have been considered key materials for future magnetoelectric storage devices. Thus, β-AsP structures with 0%–2% at vacancy concentrations (Half-metallic properties) are employed as electrode materials. Meanwhile, β-AsP at different vacancy concentrations is employed in the central scattering region to evaluate the magnetic storage performance of β-AsP as electro-logic devices (Figure S5, Supporting Information). Comparing the SFE of different configurations at all concentration vacancies, they are up to 100% and can easily achieve perfect spin current filtering as shown in Figure S6 (Supporting Information). The spin current is high in one configuration while the current in the other configuration is extremely low, and thus the giant TMR is achieved. In particular, when the vacancy concentration is 1.67%, MR is as high as $10.^{13}$

Without vacancies, since the pristine β-AsP has a large bandgap, the electrons are unable to tunnel through the barriers and show high resistance in both parallel configuration (PC) and antiparallel configuration (APC) states, which are not magnetoresistive. Whereas, with the introduction of vacancies, the barrier is lowered and the device produces high and low resistance states under the control of the magnetic field, resulting in magnetoresistance. In particular, consistent with the previous electronic structure analysis, the device current is significantly higher (by two orders of magnitude) at high concentrations of vacancies than at low concentrations of vacancies, exhibiting better “0” to “1” logic control (**Figure 3a–d**). Therefore, the electric control device also realizes the logic signal output of multiple resistance states (5 resistance states) under the control of multiple vacancy concentrations (Figure 3e). To illustrate the mechanism by which β-AsP-based magnetic memory devices achieve excellent logic control (Perfect SFE and high TMR shown in Figure 3e–g), the transport spectrum of the devices is further analyzed as shown in Figure S7 (Supporting Information). At low concentrations of vacancies, the current is completely suppressed due to the absence of transport channels. At high concentration vacancies, transport channels appear within the transport window and thus current flows through the device. Changing the magnetic field, the transport channels move beyond the transport window, and thus the current disappears. For further information, see Section S5 of the Supporting Information.

A spin-caloritronic logic device based on vacant β-AsP is designed considering nanodevice waste heat energy recovery (Figure S8, Supporting Information). The device performance is found to be significantly tuned by varying the electrode's temperature or temperature difference. Furthermore, the device exhibits a pure charge current at low concentration vacancies, but at intermediate concentration vacancies, it exhibits both spin and charge currents, with just a specific direction of polarization current

© 2024 The Authors. Advanced Functional Materials published by Wiley-VCH GmbH
16163028, 0, Downloaded from https://onlinelibrary.wiley.com/doi/10.1002/adfm.202312830 by Karlsruher Institut F., Wiley Online Library on [13/08/2024]. See the Terms and Conditions (https://onlinelibrary.wiley.com/terms-and-conditions) on Wiley Online Library for rules of use; OA articles are governed by the applicable Creative Commons License

16163028, 0, Downloaded from https://onlinelibrary.wiley.com/doi/10.1002/adfm.202312830 by Karlsruher Institut F., Wiley Online Library on [13/08/2024]. See the Terms and Conditions (https://onlinelibrary.wiley.com/terms-and-conditions) on Wiley Online Library for rules of use; OA articles are governed by the applicable Creative Commons License

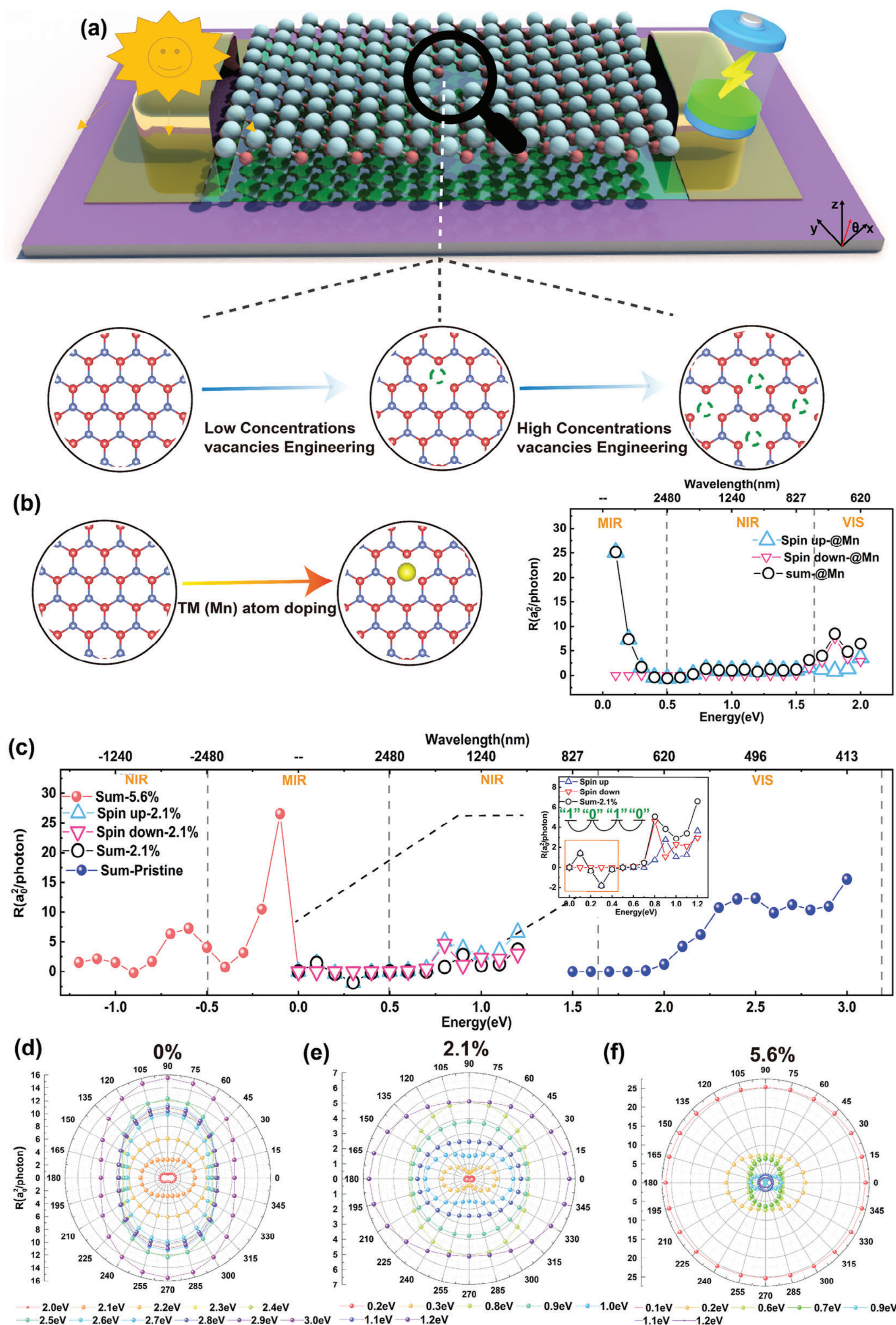

Figure 2. Simulation of optic-logic devices based on β-AsP at vacancies. a) Multi-source logic device model based on β-AsP under different vacancy concentrations. b) Maximum photocurrent as a function of photon energy for β-AsP doped with transition metal Mn atoms. c) Maximum photocurrent at different vacancy concentrations as a function of photon energies for β-AsP. d) Photocurrent as a function of polarization angle at different photon energies for vacancy concentrations of 0%; e) 2.1%; f) 5.6%.

© 2024 The Authors. Advanced Functional Materials published by Wiley-VCH GmbH

16163028, 0, Downloaded from https://onlinelibrary.wiley.com/doi/10.1002/adfm.202312830 by Karlsruher Institut F., Wiley Online Library on [13/08/2024]. See the Terms and Conditions (https://onlinelibrary.wiley.com/terms-and-conditions) on Wiley Online Library for rules of use; OA articles are governed by the applicable Creative Commons License

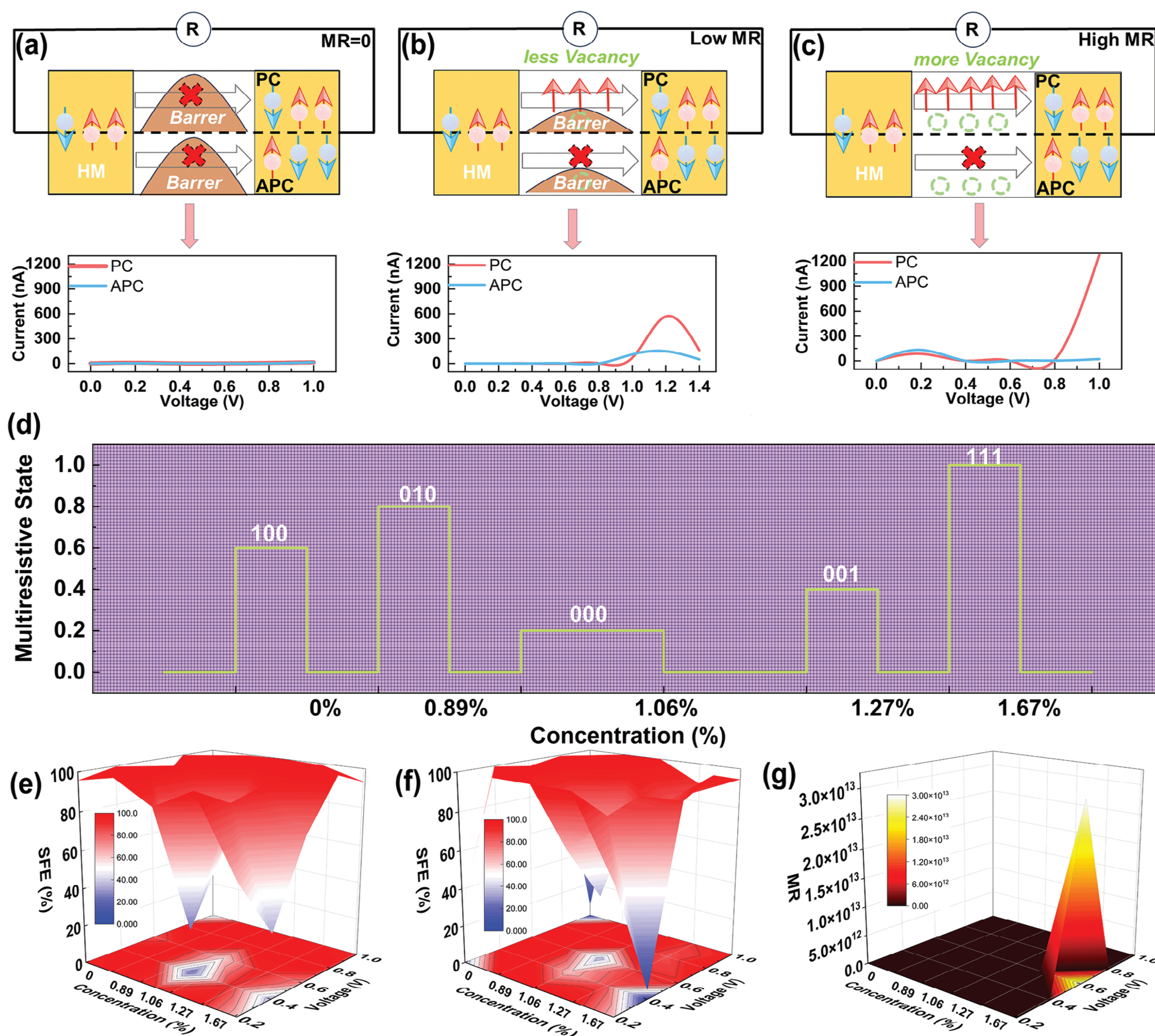

Figure 3. Electro-logic devices based on β-AsP at vacancy. Upper: Schematic diagram of the logic modulation at a) no vacancy, b) low and c) high concentrations in the PC and APC for β-AsP; Bottom: Current as a function of voltage at 0%, 1.06% and 1.27% in the PC and APC for β-AsP. d) Electrically controlled multiconfiguration logic output using β-AsP at various vacancy concentrations. Variation of spin filtration efficiency with vacancy concentration under 0–1 eV bias voltage in e) PC and f) APC for β-AsP. g) Variation of MR with vacancy concentration under 0–1 eV bias voltage for β-AsP.

going through. As a result, at vacancy concentrations of 1.06% and 1.27%, both PC and APC achieve approximately 100% thermal SFE at full temperature (Figure S9, Supporting Information). When concentration increases, the device creates spin currents in opposing directions, giving rise to the thermal spin Hall effect (**Figure** 4a–d), which can be explained by the fact that vacancies modulate A and B near the Fermi energy level. As the vacancy concentration rises to 1.06%, the energy level spread between A and B expands significantly, increasing the energy range accessible for electron jumps in a certain spin state and therefore strengthening the SFE. Increasing the vacancy concentration to 1.67% improves the coupling of spin-up and spin-down states, making it easier to generate both spin-up and spin-down currents (Figure 4e–g). By intentionally establishing a constant temperature differential between the two electrodes, the maximal value of MR is focused near a certain left electrode temperature, which decreases with increasing vacancy concentration (Figure S10, Supporting Information). On the one hand, the change of the maximum magnetoresistance with component reveals that the magnetoresistance may reach a stunning 10^{39} at low concentration vacancies (Figure 4h–i), which is the greatest HIMR value recorded thus far (Figure 4j). However, it also suggests a significant spin Seebeck effect for β-AsP in low-concentration vacancies. When the temperature differential is controlled by con-

© 2024 The Authors. Advanced Functional Materials published by Wiley-VCH GmbH

16163028, 0, Downloaded from https://onlinelibrary.wiley.com/doi/10.1002/adfm.202312830 by Karlsruher Institut F., Wiley Online Library on [13/08/2024]. See the Terms and Conditions (https://onlinelibrary.wiley.com/terms-and-conditions) on Wiley Online Library for rules of use; OA articles are governed by the applicable Creative Commons License

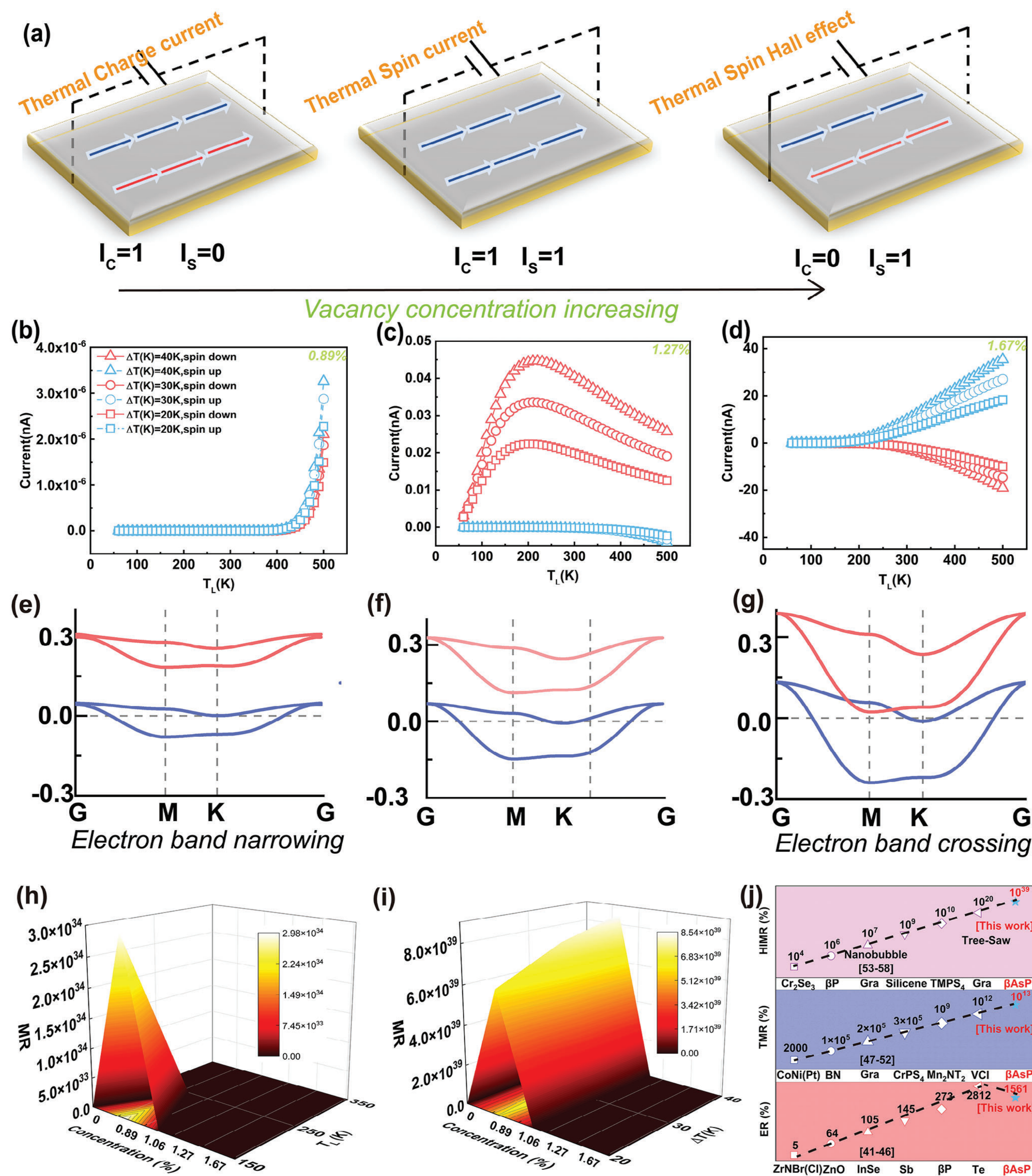

Figure 4. Thermic-logic devices using β-AsP at vacancy. a) Schematic illustration of charge current and spin current transitions in AsP thermally driven logic circuits at various vacancy concentrations. Thermal current varies with left electrode temperature (TL) at b) low (0.89%), c) medium (1.27%) and d) high concentrations (1.67%) for β-AsP at temperature variations (ΔK) of 20, 30, and 40 K. e–g) The of electron band's trend as vacancy concentration increases. Maximum magnetoresistance versus components at h) fixed ΔT and i) T_L. j) Results of ER, TMR and HIMR using nanodevices of diverse materials.[41–58]

© 2024 The Authors. Advanced Functional Materials published by Wiley-VCH GmbH

trolling the left electrode temperature, a gigantic HIMR of 1034 is obtained at a vacancy of 0.87%. This innovative thermic-logic gadget based on β-AsP under vacancy shows potential for future MRAM. For more information, read Section S6 of the Supporting Information.

3. Conclusion

In summary, electron delocalization engineering ranging from local heteroatom doping to vacancy concentration is comprehensively studied for β-AsP to achieve high-performance outputs of multifunctional by first-principles calculations and non-equilibrium Green's function method. As revealed, the As and P atomic vacancies as equivalent sites that can lead to the redistribution of β-AsP all-electrical property transition, and the interchange between the half-metallic and metallic property transitions is initially probed with varying vacancy concentrations, which is attributed to that the electronic delocalization and asymmetric electronic states contributed by the three nearest neighboring atoms of the vacancy site cause the highest occupied molecular orbital (HOMO) and the lowest unoccupied molecular orbital (LUMO) to move closer to the Fermi level and undergo spin polarization. Furthermore, the electronically controlled logic device simulations exhibit a near 100% SFE at full concentration, and 10^{13}% TMR is obtained at high-concentration vacancies. Up to 10^{39}% HIMR is available by controlling the temperature difference and electrode temperature, achieving a conversion of pure charge current to pure spin current, which is the highest records to date. This work suggests that electronic delocalization is capable of encoding logical digital information with "0" and "1" creativity for satisfying future diversified logic nanodevices.

Supporting Information

Supporting Information is available from the Wiley Online Library or from the author.

Acknowledgements

F.L. and T.W. contributed equally to this work. This project received funding from Alexander von Humboldt Foundation, National Natural Science Foundation of China under Grants (No. 11704291; 21972164; 22279161), Hubei Province Key Laboratory of Systems Science in Metallurgical Process (Wuhan University of Science and Technology, No. Y202101, Y202208), Scientific research project of Education Department of Hubei Province (No. 2022024), the Natural Science Foundation of Jiangsu Province (BK. 20210130), Innovative and Entrepreneurial Doctor in Jiangsu Province (JSSCBS20211428), and supported by High-Performance Computing Center of Wuhan University of Science and Technology. Sicong Zhu also acknowledges the support from China Scholarship Council.

Open access funding enabled and organized by Projekt DEAL.

Conflict of Interest

The authors declare no conflict of interest.

Data Availability Statement

The data that support the findings of this study are available from the corresponding author upon reasonable request.

Keywords

broadband response, delocalized electron, magneto-resistance, vacancy engineering, waste energy recovery

Received: October 17, 2023
Revised: February 26, 2024
Published online:

[1] P. Qin, H. Yan, X. Wang, H. Chen, Z. Meng, J. Dong, M. Zhu, J. Cai, Z. Feng, X. Zhou, L. Liu, T. Zhang, Z. Zeng, J. Zhang, C. Jiang, Z. Liu, *Nature.* **2023**, *613*, 485.
[2] H.-C. Ruiz Euler, M. N. Boon, J. T. Wildeboer, B. van de Ven, T. Chen, H. Broersma, P. A. Bobbert, W. G. van der Wiel, *Nat. Nanotechnol.* **2020**, *15*, 992.
[3] M. Hossain, B. Qin, B. Li, X. Duan, *Nano Today.* **2022**, *42*, 101338.
[4] T. Yan, F. Liu, Y. Wang, J. Yang, C. Ding, Y. Cai, Z. Wu, X. Zhan, F. Wang, Y. Tian, J. He, Z. Wang, *Adv. Electron. Mater.* **2022**, *8*, 2101385.
[5] J. Železný, P. Wadley, K. Olejník, A. Hoffmann, H. Ohno, *Nat. Phys.* **2019**, *15*, 197.
[6] R. Rojaee, R. Shahbazian-Yassar, *ACS Nano.* **2020**, *14*, 2628.
[7] Y. Lee, S. Che, J. Velasco jr., X. Gao, Y. Shi, D. Tran, J. Baima, F. Mauri, M. Calandra, M. Bockrath, C. N. Lau, *Nano Lett.* **2022**, *22*, 5094.
[8] C.-T. Yip, M. Isobe, C.-H. Chan, S. Ren, K.-P. Wong, Q. Huo, C.-S. Lee, Y.-H. Tsang, Y. Han, C.-H. Lam, *Phys. Rev. Lett.* **2020**, *125*, 258001.
[9] A. Bedoya-Pinto, J.-R. Ji, A. K. Pandeya, P. Gargiani, M. Valvidares, P. Sessi, J. M. Taylor, F. Radu, K. Chang, S. S. P. Parkin, *Science.* **2021**, *374*, 616.
[10] L. Zeng, X. Zhang, Y. Liu, X. Yang, J. Wang, Q. Liu, Q. Luo, C. Jing, X.-F. Yu, G. Qu, P. K. Chu, G. Jiang, *Chem.* **2022**, *8*, 632.
[11] G. Qu, T. Xia, W. Zhou, X. Zhang, H. Zhang, L. Hu, J. Shi, X.-F. Yu, G. Jiang, *Chem. Rev.* **2020**, *120*, 2288.
[12] B. Liu, M. Köpf, A. N. Abbas, X. Wang, Q. Guo, Y. Jia, F. Xia, R. Weihrich, F. Bachhuber, F. Pielnhofer, H. Wang, R. Dhall, S. B. Cronin, M. Ge, X. Fang, T. Nilges, C. Zhou, *Adv. Mater.* **2015**, *27*, 4423.
[13] Z.-Y. Guo, Y. Si, W.-Q. Xia, F. Wang, H.-Q. Liu, C. Yang, W.-J. Zhang, W.-W. Li, *Proc. Natl. Acad. Sci. USA.* **2022**, *119*, 2201607119.
[14] F. Liu, X. Zhang, P. Gong, T. Wang, K. Yao, S. Zhu, Y. Lu, *RSC Adv.* **2022**, *12*, 3745.
[15] C. Chen, Y. Yin, R. Zhang, Q. Yuan, Y. Xu, Y. Zhang, J. Chen, Y. Zhang, C. Li, J. Wang, J. Li, L. Fei, Q. Yu, Z. Zhou, H. Zhang, R. Cheng, Z. Dong, X. Xu, A. Pan, K. Zhang, J. He, *Nat. Mater.* **2023**, *22*, 671.
[16] R. Hu, C. Dai, C. Wang, J. Lin, H. Hu, Z. Li, H. Lin, L. Ding, Y. Chen, B. Zhang, *Adv. Funct. Mater.* **2021**, *31*, 2101660.
[17] X. Cai, Y. Chen, B. Sun, J. Chen, H. Wang, Y. Ni, L. Tao, H. Wang, S. Zhu, X. Li, Y. Wang, J. Lv, X. Feng, S. A. T. Redfern, Z. Chen, *Nanoscale.* **2019**, *11*, 8260.
[18] Z. Zhu, J. Guan, D. Tománek, *Nano Lett.* **2015**, *15*, 6042.
[19] J. Zhang, Y.-F. Zhang, Y. Li, Y.-R. Ren, S. Huang, W. Lin, W.-K. Chen, *Phys. Chem. Chem. Phys.* **2021**, *23*, 51431.
[20] H. Zhao, L. Han, B. Jia, Y. Chen, X. Guan, L. Wu, P. Lu, *Phys. Status Solidi RRL.* **2022**, *16*, 2200043.
[21] F. Wang, Z. Liu, Z. Xiang, C. Zhang, A. Lu, F. Qi, J. Tan, J.-S. Liu, *Energy Environ. Sci.* **2023**, *16*, 5154.
[22] C. Zhang, T. Zhu, S. Kahn, S. Li, B. Yang, C. Herbig, X. Wu, H. Li, K. Watanabe, T. Taniguchi, S. Cabrini, A. Zettl, M. P. Zaletel, F. Wang, M. F. Crommie, *Nat. Commun.* **2021**, *12*, 2516.
[23] J. Wang, J. Zhang, S. Duan, L. Jia, Q. Xiao, H. Liu, H. Hu, S. Cheng, Z. Zhang, L. Li, W. Duan, Y. Zhang, H. Lin, *Nano Lett.* **2022**, *22*, 8008.
[24] H. Huang, A. Cho, S. Kim, H. Jun, A. Lee, J. W. Han, J. Lee, *Adv. Funct. Mater.* **2020**, *30*, 2003889.

© 2024 The Authors. Advanced Functional Materials published by Wiley-VCH GmbH

16163028, 0, Downloaded from https://onlinelibrary.wiley.com/doi/10.1002/adfm.202312830 by Karlsruher Institut F., Wiley Online Library on [13/08/2024]. See the Terms and Conditions (https://onlinelibrary.wiley.com/terms-and-conditions) on Wiley Online Library for rules of use; OA articles are governed by the applicable Creative Commons License

[25] P. Kumari, K. P. Misra, S. Chattopadhyay, S. Samanta, *Mater. Today: Proc.* **2021**, *43*, 3297.
[26] P. Pluengphon, T. Bovornratanaraks, P. Tsuppayakorn-aek, U. Pinsook, B. Inceesungvorn, *Int. J. Hydrogen Energy.* **2019**, *44*, 21948.
[27] P. Li, T. Ding, J. Li, C. Zhang, Y. Dou, Y. Li, L. Hu, F. Liu, C. Zhang, *Adv. Funct. Mater.* **2020**, *30*, 1910059.
[28] Y. Chen, D. Huang, L. Lei, S. Chen, X. Liu, M. Cheng, *Nanoscale* **2021**, *13*, 4995.
[29] W. Zheng, K. Bian, X. Chen, Y. Shen, S. Zhang, R. Stöhr, A. Denisenko, J. Wrachtrup, S. Yang, Y. Jiang, *Nat. Phys.* **2022**, *18*, 1317.
[30] M. Du, Z. Miao, H. Li, F. Zhang, Y. Sang, L. Wei, H. Liu, S. Wang, *Nano Energy.* **2021**, *89*, 106477.
[31] J. Liu, F. Yang, J. Lu, S. Ye, H. Guo, H. Nie, J. Zhang, J. He, B. Zhang, Z. Ni, *Nat. Commun.* **2022**, *13*, 3855.
[32] Q. Yu, J. Li, J. Wu, F. Liu, Y. Zhang, H. Deng, Z. Yang, J. Zhang, C. Chen, L. Fang, S. Zhu, J. Wang, J. Leng, Z. Jiang, K. Zhang, P. Zhou, *Adv. Funct. Mater.* **2023**, *33*, 2307368.
[33] T. O. Poehler, H. E. Katz, *Energy Environ. Sci.* **2012**, *5*, 8110.
[34] J. Yang, J. Zhou, J. Lu, Z. Luo, J. Yang, L. Shen, *Mater. Horiz.* **2022**, *9*, 1422.
[35] H.-X. Xu, C. Wang, G. Hu, Y. Wang, S. Tang, Y. Huang, X. Ling, W. Huang, C.-W. Qiu, *Adv. Opt. Mater.* **2021**, *9*, 2100190.
[36] Z.-Y. Yan, K.-H. Xue, Z. Hou, Y. Shen, H. Tian, Y. Yang, T.-L. Ren, *Phys. Rev. Appl.* **2022**, *17*, 054027.
[37] G. Kresse, J. Hafner, *Phys. Rev. B* **1993**, *47*, 558.
[38] G. Kresse, J. Furthmüller, *Phys. Rev. B.* **1996**, *54*, 11169.
[39] J. Taylor, H. Guo, J. Wang, *Phys. Rev. B.* **2001**, *63*, 245407.
[40] S. Smidstrup, T. Markussen, P. Vancraeyveld, J. Wellendorff, J. Schneider, T. Gunst, B. Verstichel, D. Stradi, P. A. Khomyakov, U. G. Vej-Hansen, M.-E. Lee, S. T. Chill, F. Rasmussen, G. Penazzi, F. Corsetti, A. Ojanperä, K. Jensen, M. L. N. Palsgaard, U. Martinez, A. Blom, M. Brandbyge, K. Stokbro, *J. Phys.: Condens. Mater.* **2019**, *32*, 015901.
[41] Y. Zhang, R. Cao, Y. Hu, Y. Wang, Y. Xie, *Appl. Surf. Sci.* **2021**, *560*, 149907.
[42] S. Gao, L. Liu, B. Wen, X. Zhang, *Phys. Chem. Chem. Phys.* **2021**, *23*, 6075.
[43] Y. Hou, H. Liang, A. Tang, X. Du, Z. Mei, *Appl. Phys. Lett.* **2021**, *118*, 063501.
[44] F. Chu, M. Chen, Y. Wang, Y. Xie, B. Liu, Y. Yang, X. An, Y. Zhang, *J. Mater. Chem. C.* **2018**, *6*, 2509.
[45] S. Li, T. Wang, X. Chen, W. Lu, Y. Xie, Y. Hu, *Nanoscale* **2018**, *10*, 7694.
[46] S. Gao, C. Sun, X. Zhang, *Nanophotonics* **2020**, *9*, 1931.
[47] K. Masuda, H. Itoh, Y. Sonobe, H. Sukegawa, S. Mitani, Y. Miura, *Phys. Rev. B.* **2021**, *103*, 064427.
[48] H. Yu, Z. Shao, Y. Tao, X. Jiang, Y. Dong, J. Zhang, Y. Liu, X. Yang, D. Chen, *Phys. Chem. Chem. Phys.* **2022**, *24*, 3451.
[49] J. Yang, S. Fang, Y. Peng, S. Liu, B. Wu, R. Quhe, S. Ding, C. Yang, J. Ma, B. Shi, L. Xu, X. Sun, G. Tian, C. Wang, J. Shi, J. Lu, J. Yang, *Phys. Rev. Appl.* **2021**, *16*, 024011.
[50] B. Wang, J. Li, Y. Yu, Y. Wei, J. Wang, H. Guo, *Nanoscale.* **2016**, *8*, 3432.
[51] X. Zhang, P. Gong, F. Liu, J. Wu, S. Zhu, *ACS Appl. Nano Mater.* **2022**, *5*, 15183.
[52] Y. Feng, X. Wu, G. Gao, *Appl. Phys. Lett.* **2020**, *116*, 022402.
[53] S.-J. Zhang, J.-M. Yan, F. Tang, J. Wu, W.-Q. Dong, D.-W. Zhang, F.-S. Luo, L. Chen, Y. Fang, T. Zhang, Y. Chai, W. Zhao, X. Wang, R.-K. Zheng, *ACS Appl. Mater. Interfaces.* **2021**, *13*, 58949.
[54] C. Zheng, K. Wu, K. Jiang, K. Yao, S. Zhu, Y. Lu, *Phys. B* **2022**, *626*, 413580.
[55] Y. Ni, G. Deng, J. Li, H. Hua, N. Liu, *ACS Omega* **2021**, *6*, 15308.
[56] T. Wang, B. Liu, S. Liu, S. Zhu, Y. Lu, *Phys. E* **2023**, *146*, 115529.
[57] X.-J. Gao, P. Zhao, G. Chen, *Chem. Phys. Lett.* **2018**, *699*, 250.
[58] Y.-Z. Lv, P. Zhao, *Chin. Phys. Lett.* **2019**, *36*, 017301.

© 2024 The Authors. Advanced Functional Materials published by Wiley-VCH GmbH

16163028, 0, Downloaded from https://onlinelibrary.wiley.com/doi/10.1002/adfm.202312830 by Karlsruher Institut F., Wiley Online Library on [13/08/2024]. See the Terms and Conditions (https://onlinelibrary.wiley.com/terms-and-conditions) on Wiley Online Library for rules of use; OA articles are governed by the applicable Creative Commons License